A Monolithic Integrated Light-Emitting-Diode/Photodetector Sensor for Photoactive Analyte Monitoring: Design and Simulation

Peyman Amiri and Matthias Auf der Maur*
Department of Electronic Engineering, University of Rome Tor Vergata, Rome, Italy

Olga Casals and Joan Daniel Prades
Department of Electronic and Biomedical Engineering, Universitat de Barcelona, Spain

Jana Hartmann and Andreas Waag
Institute of Semiconductor Technology, Technische Universitt Braunschweig, Hans-Sommer-Strae 66, 38106 Braunschweig, Germany

Carolin Pannek and Laura Engel
Fraunhofer Institute for Physical Measurement Techniques, Freiburg im Breisgau, Germany

We present the simulation and design optimization of an integrated Light-Emitting Diode/Photodetector (LED-PD) sensor system for monitoring of light absorbance changes developing in analyte-sensitive compounds. The sensor integrates monolithically both components in a single chip, offering advantages such as downsizing, reduced assembly complexity, and lower power consumption. The changes in the optical parameters of the analyte-sensitive ink are detected by monitoring the power transmission from the LED to the PD. Ray tracing and coupled modelling approach (CMA) simulations are employed to investigate the interaction of the emitted light with the ink. In highly absorbing media, CMA predicts more accurate results by considering evanescent waves. Simulations also suggest that approximately 39% change in optical transmission can be achieved by adjusting the ink-deposited layer thickness and varying the extinction coefficient from 10^{-4} to 3×10^{-4}.

I. INTRODUCTION

The optical properties of many substances develop changes in the presence of external stimuli [1], like temperature, radiation, mechanical stress or chemical substances, both inorganic and also of biological nature. Among them, optical absorption is one of the most apparent, simple and widely used ways to track the presence of these stimuli. When optical absorption variations take place in the visible light spectral range, they can often be directly observed even with the naked eye leading to the so-called colorimetric indicators (or colorimetric inks).

In analytical chemistry, colorimetric indicators are know since more than a century and are the backbone of basic molecular recognition and quantification schemes [2]. They are so reliable and trusted that they are considered one of the golden standards to detect hazardous emissions in field operations [3]. More recently, the same principle has been extended to the recognition of molecules of interest in biology and medicine, to build quick and inexpensive diagnosis kits [4]. However, the potential of colorimetric sensing goes beyond molecular recognition. Temperature can be measured by temperature indicators behaving in many different ways, like for example continuous color changes to measure continuous temperature values, or discrete changes triggered at specific temperature thresholds either reversibly or non-reversibly. They are applied as cost effective temperature indicators in cold-chain monitoring [5] and as counterfeiting measures [6]. Similarly, color changes have been used to fingerprint the exposure to non-visible radiation, and to build from UV to highly-ionizing-radiation dosimeters [7]. Even mechanical stimulus can be detected by means of colorimetry, to quantify and map strain in engineering structures [8] or as anti-tampering indicators in packaging [9]. Therefore, the possibility of monitoring continuously the signal of colorimetric indicators is of interest in many fields of sensing and instrumentation.

There exist a broad literature that describe different arrangements to measure these color changes in more or less convenient and sensitive setups [10, 11]. Most of them consist of a light source, a light detector and an optical path where light is allowed to interact with the colorimetric indicator (in the following, we will refer to it indistinctly as indicator, ink, or sensitive layer). Changes in the physical and chemical properties of the sensitive layer affect the transmitted electromagnetic field from the light source to the detector, enabling monitoring of alterations in the optical parameters of the sensitive layer. Therefore, maximizing sensitivity usually involves maximizing the optical path of interaction of the light with this layer. This method has facilitated the design and fabrication of a wide range of sensors [12–14]. Optical spectral selection (i.e. the light variations are mostly measured at the wavelength where the ink develops most of its optical changes) is either made at the emitter side (with sharp band emitters like Lasers, narrow band emitters like LEDs, or employing filters) or at the detector

* auf.der.maur@ing.uniroma2.it

side (using filters in most of the cases). Also, interfering effects like variations of the light emission, differences in the optical alignment of individual devices or degradation over time of the optoelectronic performance of either the emitter or the detector pose challenges on the stability and repeatability of this type of measurement system.

A common challenge in utilizing micro-scale LEDs in sensory applications is the requirement of an external photodetector and its alignment. Moreover, incorporating an external detector on top of the micro LEDs, as seen in previous designs [13, 14], could complicate the deposition of the ink and potentially restrict the interaction of the ink with the analyte. A possible path to improve these aspects is the microelectronic integration of the optoelectronic components into a single substrate [15]. First, miniaturization offers the possibility of incorporating multiple measurement channels (i.e. LED-PD pairs) to integrate the measurement of multiple inks at once, or to add reference channels for signal compensation, without increasing significantly system. Second, microelectronic processing offers the highest standards of geometry definition and repeatability, that minimizes the differences due to optical miss-alignment of the components. Third, smaller form factors possibly contribute to minimizing the light intensity needed and thus the electrical power consumption. This effect, however, can also be detrimental for the system sensitivity due to the shorter optical path, if appropriate measures are not applied. For all these, the monolithic integration of LED-PD systems applied to colorimetric sensing is very promising, but not straightforward, and therefore requires specific studies investigating and optimizing the complex optical propagation taking place in the system.

Among the different optoelectronic materials suitable for operation in the visible range, III-nitrides and especially GaN and its alloys have attracted considerable attention in the research community due to their exceptional properties, including high brightness, low energy consumption, and stability [16–18]. From the point of view of applications, its high efficiency at short visible wavelengths turned it into the primary material for solid state lighting by means of down conversion schemes. But the applications of GaN optoelectronic devices extend beyond solid-state lighting [18]. Various devices have emerged utilizing GaN technology, such as sensors [13], optical communication systems [19], and microdisplays [20]. For instance, in [21], an integrated visible light communication system was designed and fabricated based on InGaN/GaN multiple-quantum well diodes. Suspended waveguides were employed to optically couple the transmitter and the detector, achieving full-duplex communication on the same channel. This was made possible by leveraging the dual functionality of the p-n junction InGaN/GaN multiple-quantum well diode as both a light emitter and a photodetector. Also, it is a very capable semiconductor in special applications requiring high-power and high-speed. For all this, GaN is often referred to as the second-Silicon. In regards to the integration of colorimetric interrogation systems operating in the visible range it appears like an excellent candidate.

In this study, we present optical simulations of an integrated GaN LED-photodetector (LED-PD) system design to interrogate the optical changes developing in colorimetric sensitive layers. Two distinct optical devices are formed through etching of a standard blue-emitting InGaN/GaN LED wafer, leading to an extremely simple monolithic configuration. We considered two configurations. A first one, where the analyte-sensitive ink is deposited in the gap between these electrically isolated devices, with one device operating as an LED and the other as a PD. A second one, where the ink coats the backside of the device. A ray tracing model coupled with wave optics is employed to investigate the interaction of emitted light with the ink. Additional simulations are performed to optimize the sensitivity and power transmission of the sensor design, leading to a set of design recommendations.

II. DETECTOR DESIGN

A schematic diagram depicting the designed structure is presented in Fig. 1. A commercially available InGaN/GaN blue-emitting multi-quantum well (MQW) LED epitaxial structure fabricated on a sapphire substrate was utilized in our experimental implementation and considered in the simulations. Through etching, two distinct devices were formed by removing all layers down to the n-GaN layer, creating a gap between them. To complete the fabrication of these two electro-optic active regions, electrical contact metalizations where deposited on the common n region and the independent p regions of each device. Only the p-side metalizations are relevant for the simulations since they lay on top of the junction regions of LED and the PD (the common n-side contact is deposited further away, far from the optically active region). This gap was subsequently filled with an analyte-sensitive ink using spin coating. However, to prevent electrical contact between the ink and the semiconductor, as well as to passivate the surface, an SU-8 epoxy-based photoresist layer was deposited first.

To achieve the desired functionality, one of the diodes can be electrically biased to operate as an LED, while the short-circuit current of the other diode can be measured, acting thus as a detector. As both devices are identical, either of them can serve as both an LED and a PD, in principle.

The emitted light from the LED propagates in all directions, with a fraction of it expected to interact with the ink and eventually be absorbed by the detector. By monitoring the photocurrent of the detector, which is directly proportional to the optical power transmitted from the LED to the active MQW layer of the detector, it becomes possible to detect changes in the ink along the optical paths. These changes occur due to the interaction between the sensitive ink and the external target (either

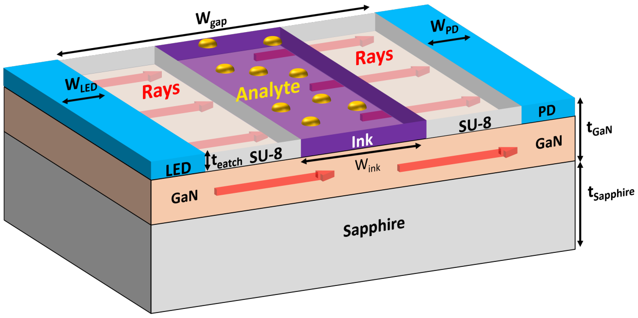

(a)

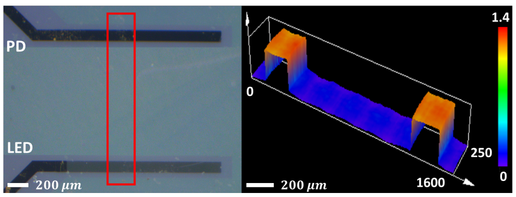

(b)

FIG. 1: a) Schematic diagram of an LED-PD based integrated sensor. The blue regions inidcate the GaN/InGaN MQW stacks forming the active region of the devices. The analyte in contact with the ink (purple) is shown in yellow. The red arrows indicate schematically the optical transmission from the LED to the PD. b) An optical image of a real device and a 3D profile measured with a Confocal Laser Scanning Microscope LEXT OLS5000.

a chemical analyte or a physical stimulus, as discussed in the introduction).

The selection of the optimal wavelength is mostly determined by the properties of the ink. Notably, the changes in optical absorption are not uniform across all wavelengths, but they depend on the properties of the sensitive layer and analyte [22, 23]. To enhance sensitivity, it is essential to choose a wavelength within the range where the ink's absorption coefficient undergoes maximum changes. The tunability of the InGaN LED's emission peak, achieved mainly through adjustments in material composition [24, 25], provides a means to optimize the alignment between operating wavelength and the ink's optical properties. In this investigation, the utilized ink exhibits increased sensitivity within the 420–450 nm wavelength range (Fig. S2), while based on Fig. S1 the emission peak of the blue LED is around 450 nm, which is precisely where InGaN LED technology exhibits its peak electro-optic conversion efficiency, and the overlap between emission and absorption peaks at 430 nm. This alignment not only leverages the inherent sensitivity of the ink but also mitigates optical losses, thereby enhancing the overall efficiency of the system.

III. MODELING APPROACH

Numerical simulation has been proven to be an effective tool to predict performance of integrated electronic systems and enable designers to optimize the corresponding parameters to archive the desirable performance [26]. Since the geometry and dimensions of the layers are considerably larger than the wavelength of the emitted light of around 450 nm in vacuum for the studied devices, a geometrical optics approach has been chosen to avoid the excessive computational cost of solving Maxwells equations. Moreover, it allows for a simpler treatment of the spatially distributed incoherent light source. Specifically, the ray tracing module of COMSOL has been used to study the light propagation from the LED to the detector and the interaction with the analyte-sensitive ink. COMSOL Multiphysics Ray-tracing package offers a simulation platform for electromagnetic wave propagation using the ray tracing approach in 2D and 3D geometries [27].

Initially, a 2D geometry shown schematically in Fig. 2 has been created using the data in Table I, and material parameters have been set according to Fig. 2 and Table II. To model the emission of the light in the ray tracing approach, several light sources with spherical and uniform emission patterns have been added inside the LED's MQW layers. It is also assumed that the MQW layer on the detector side is a perfect absorber that absorbs all the rays reaching the active detector volume. By monitoring the absorbed power in the detector, which is proportional to the detector's short circuit current, it would be possible to track changes in the optical parameters of the medium between the LED and the detector.

At the material discontinuity between two different media, refracted rays propagate in the directions given by Snell's equation:

$$\theta_t = \arcsin(\frac{n_i}{n_t}\sin(\theta_i)) \tag{1}$$

where n_i and n_t represent the refractive indices and θ_i and θ_t the propagation angles of the incident and transmitted rays, respectively. In a non-absorbing medium with an extinction coefficient k of zero, the propagation angles θ_i and θ_t take real values. In a weakly absorbing medium, where the power carried by each ray decreases gradually over a length scale much larger than the wavelength, it is sufficient to consider only the real part of the refractive index. Absorption of light occurs primarily when the ray travels within an absorbing medium. However, in strongly absorbing mediums, a modified version of Snell's law and the Fresnel equations must be employed. In these cases, the imaginary part of the refractive index, which represents absorption, becomes more significant, and the standard equations may not accurately predict the behavior of light at material interfaces.

To gain a more comprehensive understanding of the proposed device, a Coupled Modelling Approach (CMA) is necessary, similar to the methodology described in [28].

Parameter	Value [μm]	Parameter	Value [μm]
W_{LED}	200	t_p	0.3
W_{PD}	200	t_{MQW}	0.6
W_{gap}	1000	t_n	3.64
W_{ink}	500	t_u	3.2
t_{etch}	1.2	t_{GaN}	7.74
t_{metal}	0.1	$t_{sapphire}$	430

TABLE I: Parameters corresponding to Fig. 2

Materials	Refractive index
GaN	2.48
Sapphire	1.77
Ink	1.4
SU-8	1.6

TABLE II: Refractive index of the materials at $\lambda_0 = 450$ nm.

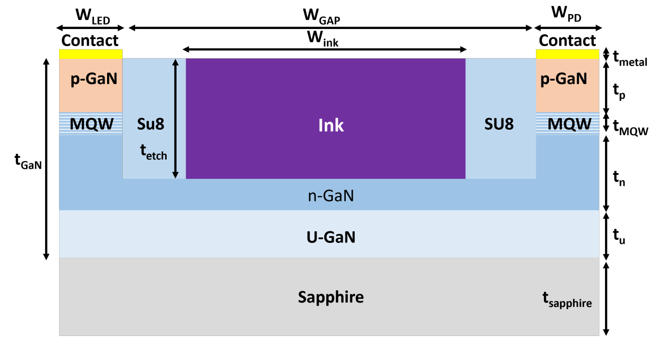

FIG. 2: Schematic of the LED-PD chemical sensor (not in scale).

This approach combines ray tracing and wave optics to accurately calculate the reflection of light at interfaces involving strongly absorbing layers. For this purpose the Wave Optics module of Comsol was employed to model the interface between two layers: a semi-infinite GaN layer and an ink layer with significant extinction coefficient. A plane wave with varying incident angles and polarizations was applied to the interface. Reflection and transmission for TE and TM polarization are plotted in Fig. S3-a and Fig. S3-b in the supplemental document. When incident waves have an angle greater than the critical angle, total reflection takes place, meaning that all the power is reflected back and no transmission occurs. However, this behavior changes when the ink layer exhibits non-negligible extinction coefficient. In this case, the reflectance becomes smaller than unity. When considering both TE and TM polarizations, the larger value of extinction coefficient in the ink layer results in a decrease in the reflection coefficient. Specifically, for incident angles near the critical angle ($\theta_c \approx 35$) and an ink extinction coefficient of 10^{-3}, only 80% - 90% would reflect from the interface. This effect can be explained by the evanescent waves, i.e. the exponentially decaying tail of the electromagnetic field of the incident wave penetrating into the ink, which suffer absorption.

The absorption caused by evanescent waves is determined by the extinction coefficient of the ink and the penetration length of the electromagnetic field. The penetration length, in turn, depends on factors such as the angle of incidence and the refractive index of the layers involved. Fig. S3-c in the supplemental document illustrates the distribution of the electric field obtained from the full-wave calculation at an incident angle of 45. In this figure, the presence of the evanescent field is visible in the ink layer near the interface with GaN.

IV. SIMULATION RESULTS

In the following subsections, we present simulation results obtained using Ray tracing and CMA (details to follow). After thoroughly comparing the two simulation approaches, the model is further developed to study more realistic conditions regarding the ink deposition pattern and spatial non-uniformity in the change of the ink's dielectric properties. An alternative Bottom configuration will be also introduced, and the corresponding results discussed.

A. Ray Tracing

Ray tracing simulation results of the proposed sensor are plotted in Fig. S4 in the supplemental document. The light sources are assumed to emit unpolarized rays with spherically uniform intensity distribution from the MQW layer on the LED side (red dots in Fig. S4-a). Initially, these rays propagate in all directions. However, since the top metal contact of the LED is relatively thick and thus assumed to have high reflectivity, rays will not be transmitted into the air. In addition, rays that travel in opposite directions of the PD and those which hit the bottom of the sapphire isubstrate are assumed to be either absorbed or scattered. In order to have a clearer picture of the propagation paths of the rays from the LED to the detector, in Fig. S4-d only the rays that reach the detector are shown.

Ray tracing simulations reveal that a large portion of the light is guided inside the GaN layer due to the refractive index contrast, and rays can reach the detector's active MQW layers and be absorbed after several reflections at the interface between GaN and sapphire, ink, and SU-8. There is also direct propagation of rays from the LED to the detector through the SU-8 and ink layers. Despite direct transmission having lower power compared to guided rays, these rays have the most interaction with the ink and these rays will play a key role in designing a small-scale integrated optical sensor. Direct rays will travel inside the ink, so that the effective interaction distance is proportional to the width of the ink region. In contrast, guided rays will travel mostly inside the GaN and interact with the ink only at the interface of the GaN and ink during reflections.

B. Coupled Modelling Approach

Wave optic simulation results have been used to modify the interaction of the rays with the GaN-ink interface according to CMA, as described in section III. Reflection and transmission from this interface for a given ink extinction coefficient are calculated using the results of wave optic simulations. By linking these results to the ray tracing model via angle-dependent boundary conditions, it is possible to implement absorption due to evanescent waves in the ray tracing simulation.

Since the variation of the ink's extinction coefficient due to the presence of a specific target analyte is proportional to its concentration, the latter is encoded in the optical power transmitted to the detector. In Fig. 3 the transmitted power to the detector has been plotted against the ink's extinction coefficient. In this figure, we compare the results obtained using only ray tracing with the one of the combined full-wave/ray tracing approach. In the ray tracing approach absorption of the light only occurs when the rays propagate inside a lossy medium, like the ink in our case. Therefore, only the direct transmission through the ink layer suffers from absorption and is useful for detection of differences in extinction coefficient. For increasing extinction coefficient of the ink, all the rays that are transmitted through the ink are absorbed, while the rays guided in the GaN layer via total reflection remain unaltered, so that the transmission levels off. In the coupled model, on the other hand, absorption due to evanescent waves increases with increasing extinction coefficient of the ink, reducing the transmission also for the guided waves.

These results indicate that for ray tracing simulations of such types of systems linking of wave optic calculations for the correct treatment of reflection at relevant interfaces is necessary. In particular, ray tracing-only simulation leads to qualitatively and quantitatively inaccurate results, which impedes its use for device optimisation. It is worth noting that the absorption threshold, where transmission starts to decay, is influenced by both the wavelength and the width of the ink layer. The wavelength is usually predefined based on LED technology and the sensitive layer, while the width of the ink layer, denoted as W_{ink}, can be adjusted to modify the threshold value. As the total optical path within the ink layer increases, currently set at 500 nm, it is expected that threshold value shifts toward lower extinction coefficients.

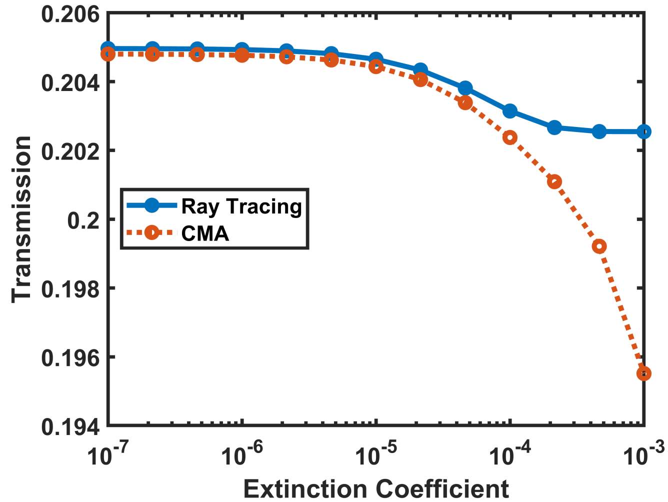

FIG. 3: Transmission from the LED to the PD as a function of ink extinction coefficient, for ray tracing only (blue) full line) and Coupled Modelling Approach (red dashed line).

C. Dependence on ink deposition pattern

Deposition of the ink on the device is done employing spin coating. Experimentally it is observed that instead of completely filling the etched well between the LED and the PD, the ink will coat the surfaces. Note that here and in the following we used a range of extinction coefficients compatible with measured data obtained from an ink sensitive to carbon monoxide.

In Fig. 4, a model where the ink entirely fills the etched region, and another model where the ink adheres to the surfaces only are compared. In the former, rays travel a longer distance in the lossy ink. In the more realistic structure, on the other hand, the optical path in the ink is shorter and less light is absorbed. This explains why transmission is only 0.22 in the fully filled case, while in the more realistic case transmission exceeds more than 0.6. A longer optical path will contribute to higher sensitivity to changes in absorption of the medium, however. As presented in Fig. 4, in the fully filled case transmission drops from 0.22 to 0.02, which corresponds to more than 90% decrease in transmitted power. In the partially filled case, on the other hand, only a 49% change in transmission is observed as transmission decreased from 0.63 to 0.32. This suggests higher sensitivity could be achieved with a fully filled trench. This, however, is only true if the changes in the absorption of the sensitive layer is spatially homogeneous.

Realistically, the changes in the ink's extinction coefficient are not homogeneous. Instead, near the surface the interaction with the analyte is much larger, and can be expected to decay with distance from the surface. To include this in the simulations, we assumed an exponential decay of the interaction strength and thus of the modification of the extinction coefficient, using the following

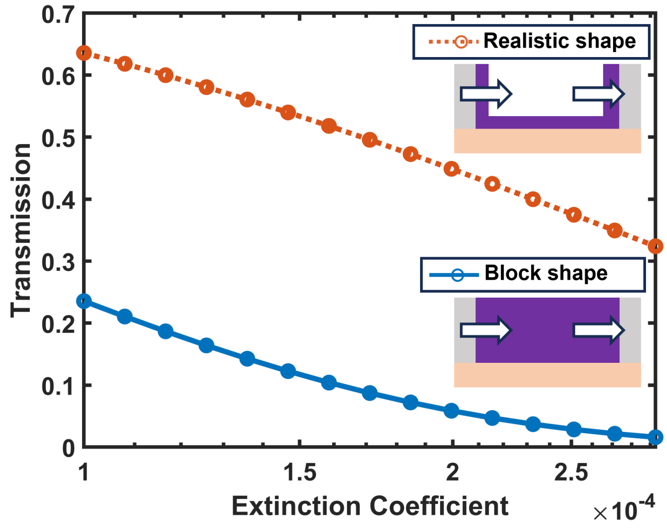

FIG. 4: Effect of ink's deposition pattern on the direct transmission of light from the LED to the PD.

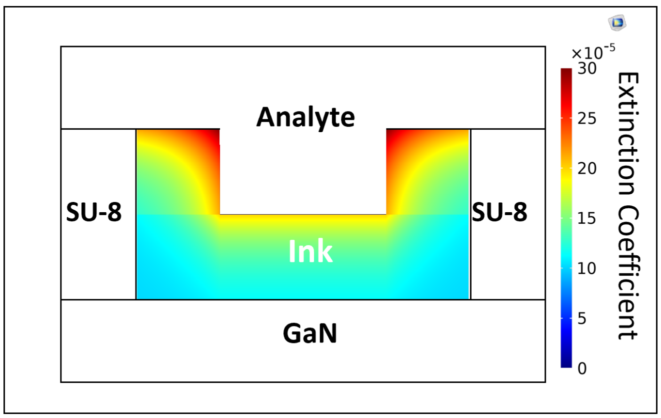

FIG. 5: Nonuniform extinction coefficient inside the ink (not in real scale)

empirical model:

$$k_{\text{ink}} = k_0 + k_1 e^{-d/\delta}, \tag{2}$$

where k_{ink} is the local value of the ink extinction coefficient, k_0 is the unperturbed nominal value for the ink, k_1 is the coefficient corresponding to the maximum changes of k, d is the distance from the surface, and δ is the characteristic decay length of the interaction. Using equation 2 results in an inhomogeneous absorption for the ink as shown in Fig. 5.

Both parameters δ and k_1 depend on the details of the interaction of the ink with the specific analyte, and directly affect the transmission of the light and therefore device sensitivity. This has been studied using ray-tracing simulation, and for simplicity only direct transmission of the rays to the PD are included in this case.

While the characteristic interaction distance δ is an intrinsic feature of the material, the ink thickness t_{ink} can be modified by adjusting the deposition process. By

$t_{\text{ink}} \setminus \delta$	0.01 μm	0.1 μm	1 μm
400 nm	28.58%	31.05%	56.67%
900 nm	26.20%	39.38%	62.14%
1100 nm	< 0.1%	27.69%	85.43%

TABLE III: Drop in transmission corresponding to Fig. 6

varying t_{ink}, it is therefore possible to modify the sensitivity of the device in terms of the transmission, as shown in Fig. 6. In particular, if t_{ink} is too large, then sensitivity decreases unless δ is large also, since most of the light travels through unaffected ink. If it becomes too thin, on the other hand, most of the light will not travel through the horizontal ink layer, and most of the effect is due to the ink on the side walls only.

Table III summarizes the calculated drop in transmission of all cases from Fig. 6. For large values of $\delta \geq 1$ μm, the change in absorption coefficient in the ink is relatively uniform. In this case, the highest drop in transmission of 85.43% would be achieved for the fully filled case (model A), as discussed before. If the characteristic interaction distance δ is smaller than t_{ink}, a change in transmission between 25% and up to above 35% is predicted, as long as the ink thickness does not exceed approximately 1μm. For small δ, where changes in the ink's absorption coefficient are limited to close proximity of the ink/analyte interface, a proper alignment between the emitting MQW layers and the sensitive portion of the ink as in model B is beneficial, leading to the peak of 39.38% reported in Table III.

D. Bottom Configuration

In this section, an alternative configuration for monitoring changes in ink extinction coefficient is considered. The design depicted in the schematic diagram in Fig. 7 closely resembles the one discussed in Section II. This configuration comprises a GaN LED positioned on a sapphire layer, with a central etch down to the n-type layer, thereby creating a pair of LED and PD . However, the analyte-sensitive ink is deposited on the back surface of the sapphire layer. In this case, the light-ink interaction happens at the interface between the ink and the sapphire substrate, without direct transmission through the ink. It is expected that a portion of rays that interact with the ink would be reflected toward the PD. To minimize direct transmission of light from the LED to the PD, incorporation of a light-blocking layer (LBL) is considered, which fills the gap between the two components. Ray tracing simulations and CMA are utilized to model the transmission of light to the PD and assess its sensitivity to variations in ink extinction coefficient. Fig. 8 illustrates the power transmission from the LED to the PD using both a ray tracing approach and the CMA, while also comparing the impact of removing the sapphire sub-

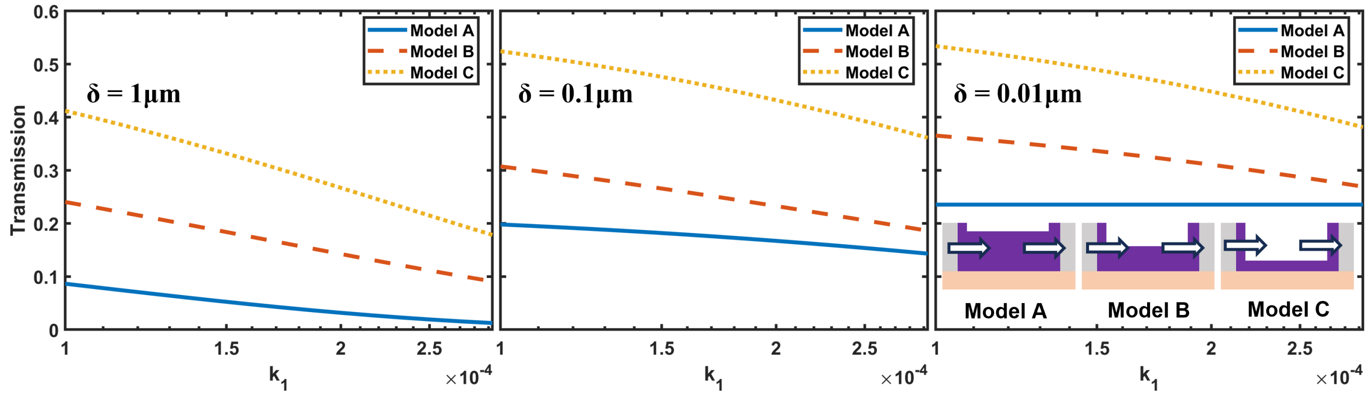

FIG. 6: The direct transmission as a function of coefficient corresponding to the maximum changes of the extinction coefficient (Eq. 2), ink deposition pattern (thickness $t_{\rm ink}$) and characteristic interaction distance δ. The $t_{\rm ink}$ for models A, B and C are 1100 nm, 900 nm and 400 nm, respectivly. Here only direct transmission of the rays from LED to the PD are included.

strate. The propagation of rays involves two main paths: guided modes within the GaN layer and reflection from the interfaces of sapphire-ink or ink-air. The presence of the sapphire layer acts as a barrier between GaN and the ink, limiting the ability to detect changes in the extinction coefficient. Consequently, only the reflected rays from the sapphire-ink and ink-air interfaces are affected by the extinction coefficient. However, when the sapphire layer is removed, the ink and GaN layers share a common interface, enabling the guided mode rays to interact with the ink through evanescent waves. As discussed in previous sections, the CMA is employed to account for the effects of evanescent waves, and its results are compared to those obtained using the ray tracing approach in Fig. 8.

It can be easily seen that for this structure removal of the substrate is necessary to obtain a reasonable sensitivity. Overall sensitivity is lower than in the former structure, although optimization might improve the results presented here. Specifically, the removal of the sapphire substrate is possible by means of Laser-Lift-off methods.

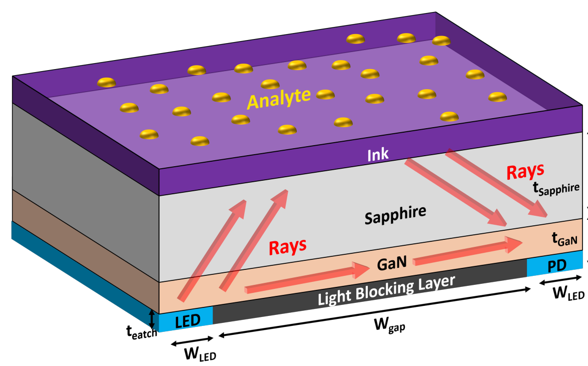

FIG. 7: Schematic diagram of the bottom configuration LED-PD based integrated sensor.The blue regions indicate the GaN/InGaN MQW stacks forming the active region of the devices. The analyte in contact with the ink (purple) is shown in yellow. The red arrows indicate the schematically the optical transmission from the LED to the PD.

V. CONCLUSIONS

We present simulation and design optimization of an integrated optoelectronic sensor for monitoring the optical changes in colorimetric indicators. The sensing device combines both the light emitter and the photodetector components on a single monolithic chip, examplified with InGaN/GaN MQW micro-LEDs structures, but extendable to other optoelectronic semiconductor technologies to cover other optical wavelengths beyond the visible. From a fundamental point of view, the color-readout devices are designed to reveal changes in the complex refractive index of a colorimetric ink due to interaction with a target analyte. This is accomplished by monitoring the power transmission from the LED to the photodetector. Numerical simulations combining ray-tracing and full-wave treatment of the interface with the ink have been used to study and optimize the device structure. While the results of these two modeling approaches are identical in low-loss mediums, in highly absorbing media, CMA predicts more accurate results. Ink deposition pattern is also found to be a key parameter in sensitivity and should be carefully adjusted. The Bottom Configuration of the sensor is also simulated, but it requires further optimizations.

Although a direct quantitative comparison with experimental data is difficult at present due to the approximations in the simulation model and uncertainties in material parameters and structural details related to the ink, the simulation results appear in line with measured changes in transmission of up to some tens of percentage points, and thus in between the results of the fully and

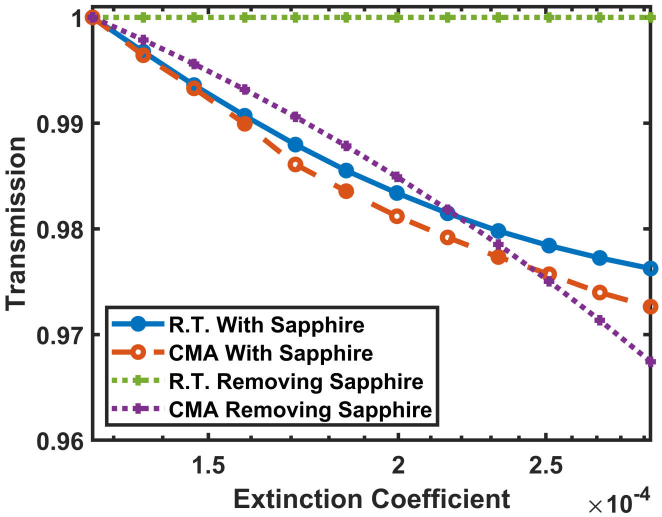

FIG. 8: Normalized transmission from the LED to the PD in the alternative configuration as a function of ink extinction coefficient and comparing results of the ray tracing simulation and the CMA.

partially filled models.

In summary, our simulations, accompanied by feasibility checks, show that the device architecture discussed here is feasible but requires considering the complex optical interplay between high refraction index layers to attain the expected functionalities and performances in future designs.

ACKNOWLEDGEMENTS

This work was funded by European Unions Horizon 2020 research and innovation program under grant agreements no. 952135 SMILE, no. 951774 FOXES and by Eurostars E! 114434 SmartFire. J.D. Prades acknowledges the support of the ICREA Academia program

DISCLOSURES

The authors declare no conflict of interest.

DATA AVAILABILITY STATEMENT

The simulation files used in this study are available upon request.
See Supplement 1 for supporting content

VI. REFERENCES

[1] Y. Foelen and A. P. Schenning, Optical indicators based on structural colored polymers, Advanced Science **9**, 2200399 (2022).

[2] Y. Fan, J. Li, Y. Guo, L. Xie, and G. Zhang, Digital image colorimetry on smartphone for chemical analysis: A review, Measurement **171**, 108829 (2021).

[3] E. Battaglia, J. Jensen, J. Jensen, D. Packard, and M. Mirotznik, Automation platform for remote use of colorimetric chemical sensors, in *Chemical, Biological, Radiological, Nuclear, and Explosives (CBRNE) Sensing XXIII*, Vol. 12116 (SPIE, 2022) pp. 140–145.

[4] W. Dungchai, O. Chailapakul, and C. S. Henry, Use of multiple colorimetric indicators for paper-based microfluidic devices, Analytica chimica acta **674**, 227 (2010).

[5] W.-P. Chuang and B.-C. Hsieh, Development of a gallic acid based time temperature indicator with adjustable activation energy, Food Control **144**, 109396 (2023).

[6] X. Luo, A. Zaitoon, and L.-T. Lim, A review on colorimetric indicators for monitoring product freshness in intelligent food packaging: Indicator dyes, preparation methods, and applications, Comprehensive Reviews in Food Science and Food Safety **21**, 2489 (2022).

[7] H. Lu, J. Xie, X.-Y. Wang, Y. Wang, Z.-J. Li, K. Diefenbach, Q.-J. Pan, Y. Qian, J.-Q. Wang, S. Wang, *et al.*, Visible colorimetric dosimetry of UV and ionizing radiations by a dual-module photochromic nanocluster, Nature communications **12**, 2798 (2021).

[8] B. H. Miller, H. Liu, and M. Kolle, Scalable optical manufacture of dynamic structural colour in stretchable materials, Nature Materials **21**, 1014 (2022).

[9] V. Rouillard and M. J. Lamb, On the performance of mechanical shock indicators, Packaging Technology and Science **30**, 257 (2017).

[10] B. M. Tissue, Ultraviolet and visible absorption spectroscopy, Characterization of Materials (2002).

[11] G. M. Fernandes, W. R. Silva, D. N. Barreto, R. S. Lamarca, P. C. F. L. Gomes, J. F. da S Petruci, and A. D. Batista, Novel approaches for colorimetric measurements in analytical chemistry–a review, Analytica Chimica Acta **1135**, 187 (2020).

[12] X.-d. Wang and O. S. Wolfbeis, Fiber-Optic Chemical Sensors and Biosensors (20152019), Analytical Chemistry **92**, 397 (2020).

[13] J. Glink, S. Bornemann, H. Spende, M. A. d. Maur, A. D. Carlo, J. D. Prades, H. S. Wasisto, and A. Waag, InGaN/GaN nanoLED Arrays as a Novel Illumination Source for Biomedical Imaging and Sensing Applications, in *EUROSENSORS 2018* (MDPI, 2018) p. 892.

[14] N. Franch, J. Canals, V. Moro, A. Vil, A. Romano-Rodrguez, J. D. Prades, J. Glink, D. Bezshlyakh, A. Waag, K. Kluczyk-Korch, M. Auf der Maur, A. di Carlo, and . Diguez, Nano illumination microscopy: a technique based on scanning with an array of individually addressable nanoLEDs, Optics Express **28**, 19044 (2020).

[15] K. Wu, H. Zhang, Y. Chen, Q. Luo, and K. Xu, All-silicon microdisplay using efficient hot-carrier electroluminescence in standard 0.18μm cmos technology, IEEE Electron Device Letters **42**, 541 (2021).

[16] B. Lu, Y. Wang, B.-R. Hyun, H.-C. Kuo, and Z. Liu, Color difference and thermal stability of flexible transparent InGaN/GaN multiple quantum wells mini-LED arrays, IEEE Electron Device Letters **41**, 1040 (2020).

[17] Y. Liu, K. Zhang, B.-R. Hyun, H. S. Kwok, and Z. Liu, High-brightness InGaN/GaN micro-LEDs with secondary peak effect for displays, IEEE Electron Device Letters **41**, 1380 (2020).

[18] H. S. Wasisto, J. D. Prades, J. Gülink, and A. Waag, Beyond solid-state lighting: Miniaturization, hybrid integration, and applications of GaN nano-and micro-LEDs, Applied Physics Reviews **6** (2019).

[19] X. Gao, J. Yuan, Y. Yang, S. Zhang, Z. Shi, X. Li, and Y. Wang, InGaN directional coupler made with a one-step etching technique, Semiconductor Science and Technology **32**, 065002 (2017).

[20] X. Zhang, P. Li, X. Zou, J. Jiang, S. H. Yuen, C. W. Tang, and K. M. Lau, Active Matrix Monolithic LED Micro-Display Using GaN-on-Si Epilayers, IEEE Photonics Technology Letters **31**, 865 (2019).

[21] Y. Wang, Y. Xu, Y. Yang, X. Gao, B. Zhu, W. Cai, J. Yuan, R. Zhang, and H. Zhu, Simultaneous light emission and detection of InGaN/GaN multiple quantum well diodes for in-plane visible light communication, Optics Communications **387**, 440 (2017).

[22] S. D. Kurbah, I. Syiemlieh, and R. A. Lal, Colorimetric detection of hydrogen peroxide by dioxido-vanadium (v) complex containing hydrazone ligand: synthesis and crystal structure, Royal Society Open Science **5**, 171471 (2018).

[23] A. Ashraf, M. Islam, M. Khalid, A. P. Davis, M. T. Ahsan, M. Yaqub, A. Syed, A. M. Elgorban, A. H. Bahkali, and Z. Shafiq, Naphthyridine derived colorimetric and fluorescent turn off sensors for Ni2+ in aqueous media, Scientific Reports **11**, 19242 (2021).

[24] S.-H. Baek, H.-J. Lee, and S.-N. Lee, High-performance flat-type InGaN-based light-emitting diodes with local breakdown conductive channel, Scientific Reports **9**, 13654 (2019).

[25] Z. Deng, Y. Jiang, Z. Ma, W. Wang, H. Jia, J. Zhou, and H. Chen, A novel wavelength-adjusting method in ingan-based light-emitting diodes, Scientific reports **3**, 3389 (2013).

[26] K. Xu, Silicon electro-optic micro-modulator fabricated in standard cmos technology as components for all silicon monolithic integrated optoelectronic systems, Journal of Micromechanics and Microengineering **31**, 054001 (2021).

[27] Comsol Multiphysics Simulation Software, version 6.0, www.comsol.com (2021).

[28] M. Topič, M. Sever, B. Lipovšek, A. Čampa, and J. Krč, Approaches and challenges in optical modelling and simulation of thin-film solar cells, Solar Energy Materials and Solar Cells **135**, 57 (2015).